Ocean Engineering 183 (2019) 282–293

Contents lists available at ScienceDirect

Ocean Engineering

journal homepage: www.elsevier.com/locate/oceaneng

On the sensitivity and uncertainty of wave energy conversion with an artificial neural-network-based controller

Liang Li [a], Zhen Gao [b], Zhi-Ming Yuan [c,a,*]

[a] Department of Naval Architecture, Ocean and Marine Engineering, University of Strathclyde, Glasgow, G4 0LZ, UK
[b] Department of Marine Technology, Norwegian University of Science and Technology, Trondheim, 7491, Norway
[c] School of Naval Architecture and Ocean Engineering, Jiangsu University of Science and Technology, Zhenjiang, 212003, China

ARTICLE INFO

Keywords:
Wave energy
Machine learning
Artificial intelligence
Artificial neural network
Model predictive control
Wave force prediction

ABSTRACT

This work addresses with sensitivity and uncertainty of the energy conversion of an oscillation-body wave energy converter with an artificial neural-network-based controller. The smart controller applies the model predictive control strategy to implement real-time latching control to the wave energy converter. Since the control inputs are future wave forces, an artificial neural network is developed and trained by the machine learning algorithm to predict the short-term wave forces based on the real-time measurement of wave elevation. The sensitivity of wave energy conversion with respect to wave frequency and receding horizon length are investigated. Uncertainties of the neural network that lead to the prediction deviation are identified and quantified, and their influences on the energy conversion are examined. The control command is derived inappropriately in the presence of prediction deviation leading to the reduction of energy absorption. Moreover, it is the phase deviation that reduces the energy absorption.

1. Introduction

Since the first proposal of wave energy concept (Salter, 1974), ocean waves are accepted as a prospective solution to the sustainable generation of power due to its high power density and all-day availability. The device used to harvest energy from ocean waves is known as the wave energy converter (WEC). The conversion mechanism of WEC can be briefly separated into three categories: body oscillation, pressure differential and overtopping. Evans et al. (1979) proposed the dynamic model for an oscillating-body WEC in regular waves, which was validated against model test measurement. Elhanafi et al. (2017) simulated the hydrodynamic performance of a floating-moored oscillating water column WEC, which utilized the change of air pressure in a chamber to drive a turbine. Margheritini et al. (2009) investigated the reliability and hydraulic performance of an innovative overtopping device 'Sea Slot-cone Generator'. The structure consists of reservoirs on the top of each other above the mean water level in which the water of incoming waves is stored temporarily.

Despite that WEC concepts with various types of energy extracting mechanisms have been proposed, most full-scale WEC products belong to the oscillating-body group (European Marine Energy Centre, 2018a, b; Unitied States Department of Energy, 2015). A remarkable advantage of the oscillating-body WEC is its reliable power take-off (PTO) system, e.g. a direct-drive generator or a hydraulic motor. Nevertheless, the energy harvesting efficiency of an oscillating-body WEC is sometimes unsatisfactory, especially within the off-resonance range, since the power is extracted from the inertial motion of the floater. One of the solutions to this problem is the incorporation of a controller to control the floater motion. Budal and Falnes (1980) proposed the latching control, which increases the energy absorption by locking and releasing the floater alternately. They found that one condition for maximizing energy absorption was to keep the velocity in phase with the wave excitation force. Therefore, the latching control is a kind of phase control. Babarit and Clement (2006) applied the latching control to two WEC concepts to increase the energy absorption. Their simulation results showed that the energy harvesting was greatly enhanced in both regular and irregular waves. Another phase control is the so-called declutching control (Babarit et al., 2009). The declutching control tunes the phase by switching off the PTO system at some time instants.

Early control strategies were mostly based on the assumption that the inputs (the wave force) to the controller are fully known. Since the energy absorption is increased over the entire interval concerned, such control algorithm is also called the optimal control. Apparently, the optimal control algorithm is not applicable in practice since the long-

* Corresponding author. Department of Naval Architecture, Ocean and Marine Engineering, University of Strathclyde, Glasgow, G4 0LZ, UK.
E-mail address: zhiming.yuan@strath.ac.uk (Z.-M. Yuan).

https://doi.org/10.1016/j.oceaneng.2019.05.003
Received 29 October 2018; Received in revised form 30 April 2019; Accepted 5 May 2019
Available online 16 May 2019
0029-8018/

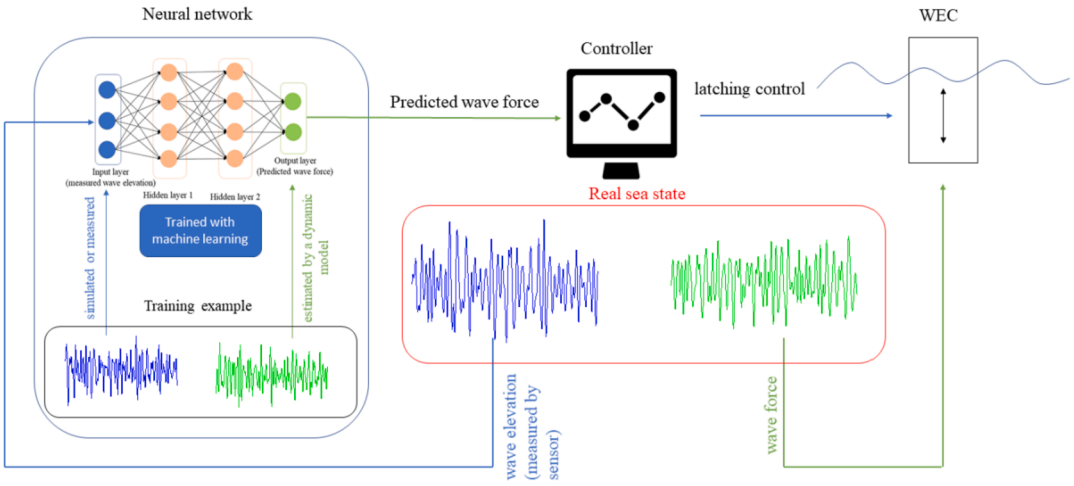

Fig. 1. The flowchart in the present research.

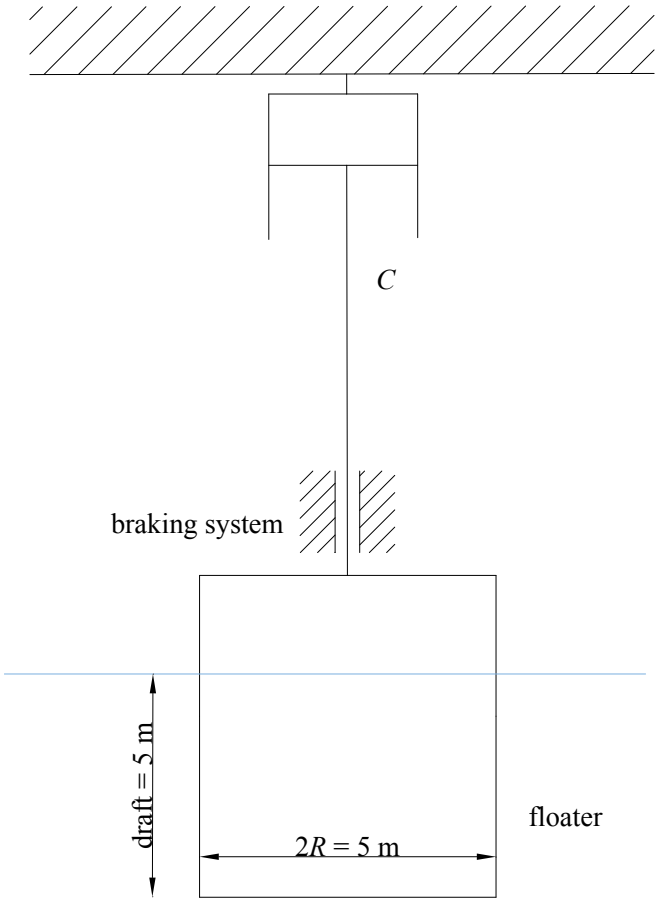

Fig. 2. Wave energy converter.

term (e.g., 1 h) wave force information is very difficult to predict. Recently, the model predictive control algorithm has been widely applied in the increase of wave energy harvesting. Instead of increased the energy absorption over the entire interval, the model predictive control seeks the optimum over a short time horizon in the future. By receding the time horizon forward step by step, the model predictive control is implemented in a real-time manner. Since the model predictive control just requires short-term wave forces over the time horizon, it shows prospect in practical application. Son and Yeung (2017a) optimized the power extraction using nonlinear model predictive control. Son and Yeung (2017b) applied the real-time optimal damping control to a permanent-magnet linear generator. Williams (2004) adopted the pseudospectral method to implement the model predictive control.

For either the optimal control or the model predictive control, the control inputs are future wave forces so that the controller becomes a non-causal system. The information of future wave force is important to the successful implementation of non-causal wave energy control (Fusco and Ringwood, 2010). Henriques et al. (2016) examined the sensitivity of real-time latching control and showed that a long prediction length is favourable. Other researchers focused on the effect of prediction error. Fusco and Ringwood (2011) proposed a frequency-domain model to investigate the effect of prediction error on the energy absorption. Zhang et al. (2016) examined the wave force error effect on optimal control in time-domain. Li et al. (2018) utilized the grey model to predict the wave forces and investigated the prediction error effect on control efficiency. They all proved that the prediction error has a negative effect on the energy absorption.

Previous researchers attempted to predict the wave forces with deterministic approaches. Ge and Kerrigan (2016) predicted the wave force using autoregressive moving average model. Halliday et al. (2011) utilized the fast Fourier transformation to predict the random sea waves. Generally, a deterministic model reads past values to predict future values. Although the deterministic forecasting method has been manifested reliable in many problems, it is still difficult to apply directly in practice. A crucial point is that it is nearly impossible to measure the wave forces with the present sensor technology since wave forces are the sum of hydrodynamic pressure on the wetted surface of the floater. Practically, only signals such as wave elevations, PTO force, and floater motion can be measured. Although it is possible to estimate the wave force based on other variables using a numerical approach (for example, a retardation function), the estimation error may be significant.

Thanks to the explosive growth of the artificial intelligence, the machine learning algorithm is being widely used for regression analysis, allowing us to predict the wave forces with other variables, e.g. the wave elevations. The application of machine learning for short-term prediction is initially seen decades ago in traffic science. Smith and Demetsky (1994) compared the neural network and nonparametric regression approaches for the prediction of the traffic flow in a highway. Yu and Xu (2014) utilized the backpropagation neural network to forecast the short-term natural gas loading at city Shanghai based on the local population. More recently, researchers begin to adopt the machine learning to improve the energy efficiency of renewable energy systems. Kalogirou (2001) presented a comprehensive review on the applications of artificial neural networks in renewable energy systems. One of the specific applications was the prediction of input to the control system. Fusco and Ringwood (2010) used the neural network to forecast the

short-term future wave excitation forces for control of WEC. Sclavounos and Ma (2018b) use the neural network to predict the future wave excitation forces and control the WEC to increase the energy conversion. Similar approach was applied by Sclavounos and Ma (2018a). Their works proved that the neural network is effective in wave excitation force prediction and can be used in the wave energy control. Nevertheless, their predictions of future wave forces were all based on the measurement of wave forces in the past. As well known, the wave excitation forces are more difficult to measure in practice so that the force-based prediction models may not work effectively in practical application. Moreover, they all assumed ideal input and the uncertainty of input to the neural network was not considered.

The present study applies the model predictive control strategy to enhance the energy efficiency of WECs and investigate the sensitivity and uncertainty of the energy absorption. To resolve the wave force prediction problem which prevents the practical application of optimal wave energy control, an artificial neural network is developed to predict the short-term wave forces using the wave elevation measurements. Moreover, the input uncertainty is considered. A numerical model for wave force estimation is also developed. Fig. 1 illustrates the workflow in this paper. Training examples are firstly generated to train the neural network with machine learning algorithm. The trained neural network measures the real-time wave elevations to predict the short-term future wave forces, which are the inputs to the controller. Based on the forecasted wave forces, the controller gives the control command to the WEC to increase the energy absorption in random sea waves.

2. Numerical model

2.1. Dynamic model of the wave energy converter

A heaving point-absorber with a nonlinear PTO system is considered in the present research (see Fig. 2). The submerged floater is a cylinder column with a radius of 2.5 m. The draft of the floater is 5 m. Only heave motion of the floater is allowed. The generator force is modeled with a linear damper C. $C = 81360$ kg/s is used. The energy absorption is improved by locking and releasing the floater alternately so that the velocity is in phase with the wave excitation force. It is known as the latching control (Budal and Falnes, 1980). The latching action is numerically modeled as a huge and finite damping force c.

Based on the impulse response theory (Cummins, 1962), the time-domain motion equation of the floater is given by

$$(M+m)\ddot{z}(t) + \int_0^t H(t-\tau)\dot{z}(\tau)d\tau + \rho g\pi R^2 z(t) = F_{wave}(t) - (C+B)\dot{z}(t) - \beta(t)c\dot{z}(t) \tag{1}$$

where M is the mass of the floater and m is the added mass at infinite frequency. $z(t)$, $\dot{z}(t)$ and $\ddot{z}(t)$ are the displacement, the velocity, and the acceleration. $B = 0.02 \times 2\sqrt{\rho g\pi R^2 (M+m)}$ (2% critical damping) is an additional damping coefficient to represent the viscous effect. $\beta(t)$ is the binary control command. When $\beta = 1$, the floater is locked; when $\beta = 0$, it is free to oscillate under the excitation of sea waves. $H(t)$ is the so-called retardation kernel function representing the radiation force, which can be obtained either from the added mass $a(\omega)$ or the potential damping $b(\omega)$. $F_{wave}(t)$ is the wave excitation force, estimated by

$$F_{wave}(t) = \mathrm{Re}\left[\sum_{j=1}^{N} \Psi(\omega_j) A_j e^{i(\omega_j t + \varepsilon_j)}\right] \tag{2}$$

where A_j, ω_j, and ε_j are the amplitude, the frequency and the random phase of regular wave component j. Ψ is the wave force transfer function.

Although Eq. (1) has been widely used as the dynamic model of a WEC, such form makes it inconvenient to implement the control strategy. An alternative model is thus developed to simulate the dynamics of the point-absorber in random waves, in which the radiation force is represented by a state-space model. The procedure is briefly introduced here and please refer to (Perez and Fossen, 2011) for more details regarding the development of the state-space model.

Denote $f(t)$ the radiation force, the following three formulas can be equivalent to each other

$$\frac{d^n f}{dt^n} + q_{n-1}\frac{d^{n-1} f}{dt^{n-1}} + \ldots + q_1\frac{df}{dt} + q_0 f = p_{n-1}\frac{d^{n-1}\dot{z}}{dt^{n-1}} + p_{n-2}\frac{d^{n-2}\dot{z}}{dt^{n-2}} + \ldots + p_1\frac{d\dot{z}}{dt} + p_0\dot{z} \tag{3}$$

$$f(t) = \int_0^t H(t-\tau)\dot{z}(\tau)d\tau \tag{4}$$

$$\begin{aligned} \dot{\vec{u}}(t) &= \vec{A}\cdot\vec{u}(t) + \vec{B}\dot{z}(t) \\ f(t) &= \vec{C}\cdot\vec{u}(t) \end{aligned} \tag{5}$$

where n is the order of ordinary differential equation Eq. (3). $\vec{u}(t)$ is a state vector with dimension $n \times 1$. $\vec{A}$, $\vec{B}$ and $\vec{C}$ are matrices with dimensions $n \times n$, $n \times 1$ and $1 \times n$. The three formulas approach to each other as $n \to \infty$. It indicates that the convolution term can be approximated by the other two methods.

Combining Eq. (3) and Eq. (5), we get

$$\vec{A} = \begin{bmatrix} -q_{n-1} & -q_{n-1} & \cdots & -q_1 & -q_0 \\ 1 & 0 & \cdots & 0 & 0 \\ 0 & 1 & \cdots & 0 & 0 \\ \vdots & \vdots & \ddots & 0 & 0 \\ 0 & 0 & \cdots & 1 & 0 \end{bmatrix}, \vec{B} = \begin{bmatrix} 1 \\ 0 \\ 0 \\ \vdots \\ 0 \end{bmatrix}$$
$$\vec{C} = [\, p_{n-1} \quad p_{n-2} \quad \cdots \quad p_1 \quad p_0 \,] \tag{6}$$

The retardation kernel function in Eq. (1) is a time-domain expression, and it can be transformed to the frequency-domain through the Fourier transformation

$$H(\omega) = \int_0^\infty H(\tau)e^{-i\omega\tau}d\tau = b(\omega) + i\omega[a(\omega) - m] \tag{7}$$

Then the rational transfer function is established to approximate $H(\omega)$

$$\widehat{H}(\omega, \boldsymbol{p}, \boldsymbol{q}) = \frac{p_{n-1}(i\omega)^{n-1} + p_{n-2}(i\omega)^{n-2} + \ldots + p_0}{(i\omega)^n + q_{n-1}(i\omega)^{n-1} + \ldots + q_0} \tag{8}$$

Parameters $\boldsymbol{p}$ and $\boldsymbol{q}$ can be estimated by the least square method. The estimation of $\vec{A}$, $\vec{B}$ and $\vec{C}$ is also called system identification (Taghipour et al., 2008).

By using the state-space representation, Eq. (1) can be re-written as

$$\begin{aligned} (M+m)\ddot{z}(t) &= F_{wave}(t) - \vec{C}\cdot\vec{u}(t) - \rho g\pi R^2 z(t) - [C + B + \beta(t)c]\dot{z}(t) \\ \dot{\vec{u}}(t) &= \vec{A}\cdot\vec{u}(t) + \vec{B}\dot{z}(t) \end{aligned} \tag{9}$$

Define a state vector $\boldsymbol{x} = [z(t),\ \dot{z}(t),\ \vec{u}(t)^T]^T$ with dimension $(n+2) \times 1$. Then Eq. (9) is re-expressed as

$$\begin{aligned} \dot{\boldsymbol{x}}(t) &= f(\boldsymbol{x}, \beta) + \boldsymbol{\eta}(t) \\ f_1(t) &= \dot{z}(t) \\ f_2(t) &= -\frac{\rho g\pi R^2}{M+m} z(t) - \frac{C + B + \beta(t)c}{M+m}\dot{z}(t) - \frac{\vec{C}}{M+m}\cdot\vec{u}(t) \\ [f_3(t), f_4(t), \ldots, f_{n+2}(t)]^T &= \vec{A}\cdot\vec{u}(t) + \vec{B}\dot{z}(t) \\ \boldsymbol{\eta}(t) &= \begin{bmatrix} 0 & \frac{F_{wave}(t)}{M+m} & \boldsymbol{0} \end{bmatrix}^T \end{aligned} \tag{10}$$

Given the initial condition $\boldsymbol{x}(0) = \boldsymbol{0}$, it becomes an initial-value problem and the floater movement histories are integrated using the

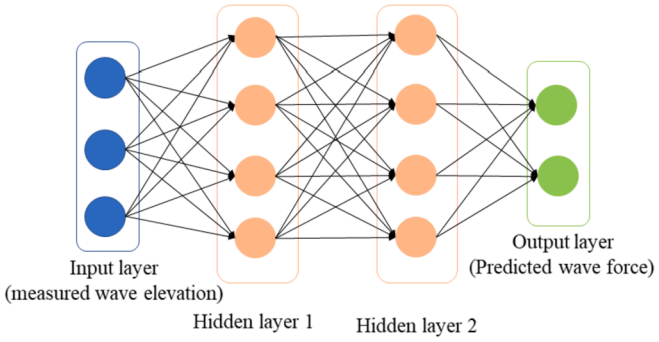

Fig. 3. Structure of a neural network.

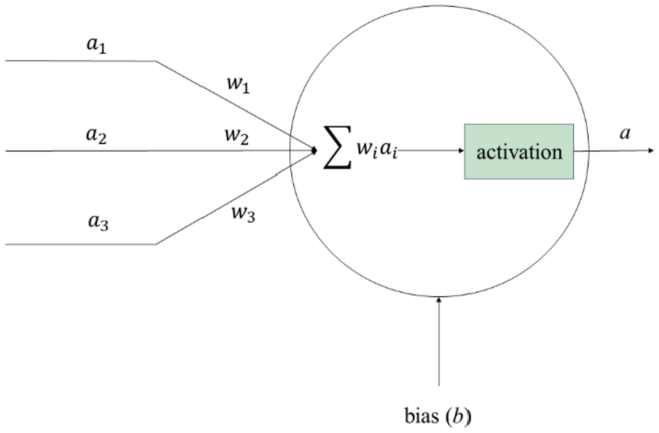

Fig. 4. The artificial neuron.

4th Runge-Kutta method. Then, the average energy absorption during simulation interval [0, T] is given by

$$P = \frac{1}{T}\int_0^T C\cdot\dot{z}(t,\beta)^2 dt \tag{11}$$

2.2. Real-time control algorithm

We aim to increase the energy absorption by applying the latching action to the floater

$$\max P = \frac{1}{T}\int_0^T C\cdot\dot{z}(t,\beta)^2 dt \tag{12}$$

That is to maximize P subject to constraint Eq. (10). We temporarily assume that the wave forces are already known and apply the Pontryagin's maximum principle (Boltyanskiĭ et al., 1956) to maximize the energy absorption. Define a Hamiltonian H:

$$H(t,\boldsymbol{x},\beta) = C\dot{z}(t)^2 + \boldsymbol{\lambda}(t)\cdot(f(t,\boldsymbol{x},\beta) + \boldsymbol{\eta}(t)) \tag{13}$$

$\boldsymbol{\lambda}$ is the Lagrange multipliers with dimension $1\times(n+2)$. The Hamiltonian reaches its maximum value on condition that

$$\beta = \begin{cases} 1 & \lambda_2 c\dot{z} < 0 \\ 0 & otherwise \end{cases} \tag{14}$$

Since the wave forces across interval [0, T] are already known, the time series of floater movement can be estimated by Eq. (10). Afterwards, the Lagrange multipliers at each time instant should be calculated. The Lagrange multipliers satisfy the following relationships.

$$\begin{aligned} &\dot{\lambda}_i(t) = -\frac{\partial H(t,\boldsymbol{x},\beta)}{\partial x_i}, i = 1,2,..,n+2 \\ &\boldsymbol{\lambda}(T) = \mathbf{0} \end{aligned} \tag{15}$$

An iterative process is applied to calculate $\boldsymbol{\lambda}$. Firstly, run the simulation with $\beta(t) = 0$ to obtain the motions and the Lagrange multipliers free of latching action. Given the Lagrange multipliers, the control command is updated by Eq. (14). Iterate the process until the updated control command converges.

Although the above procedure can derive the optimal control command, it is unable to be applied by the controller directly. This is because the control command is already determined before the dynamic process really happens. Such an off-line control is only applicable to numerical simulation whereas the control action must be implemented in a real-time manner in practice. In our work, we adopt the model predictive control strategy to control the point-absorber. Instead of seeking the optimal control command across the entire interval [0, T], the model predictive control tries to maximize the energy absorption over a finite time horizon [t, t+Δt]. Δt is the prediction horizon. In the present study, $\Delta t = 2.5$ s is adopted. By receding the time horizon [t, t+Δt] forward step by step, the real-time control is implemented. Since the energy is increased over a part of the entire interval, the model predictive control belongs to the sub-optimal control family. The application of model predictive control strategy allows us to implement the control action in a real-time manner. Moreover, the model predictive control just requires the wave forces within a short period Δt. This feature makes great sense in practice since the short-term wave forces are predictable.

3. Wave force prediction with neural network

3.1. Neural network

Fig. 3 sketches the structure of the developed artificial neural network, which is composed of an input layer, two hidden layers, and an output layer. Each layer consists of neurons to receive and send signals. For the problem in this study, the inputs are the measured wave elevation in the past and the outputs are the predicted vertical wave excitation forces over the prediction horizon [t, t+Δt]. In the present study, the predictive horizon Δt is set to 2.5 s, and the time step is 0.01 s. Therefore, totally 250 points future wave forces are predicted over the prediction horizon.

As shown in Fig. 4, the neuron processes the inputs by two sets of parameters, $\boldsymbol{w} = (w_{11}^2, w_{12}^2, \ldots, w_{ji}^k, \ldots)$ and $\boldsymbol{b} = (b_1^2, b_2^2, \ldots, b_j^k, \ldots)$. w_{ji}^k is the weight for the connection from the ith neuron in the $(k-1)^{\text{th}}$ layer to the jth neuron in the kth layer. b_j^k is the bias of the jth neuron in the kth layer. Then, the activation of the jth neuron in the kth layer is determined by the activations of all neurons in the $(k\text{-}1)^{\text{th}}$ layer:

$$a_j^k = \sigma\left(z_j^k\right), z_j^k = \sum_i w_{ji}^k a_i^{k-1} + b_j^k \tag{16}$$

where $\sigma(x)$ is the activation function. The sigmoid function ($\sigma(x) = 1/(1+e^{-x})$) is selected here as the activation function. z_j^k is the weighted input to the activation function of neuron j in layer k.

The neural network is used for the short-term wave force prediction to implement the real-time control. A remarkable advantage of the neural network technology against traditional prediction approach is that it allows us to forecast variable A with variable B. It makes senses in practice since the wave force acting on the floater is nearly impossible to measure so that the prediction cannot be based on the wave force itself. In our work, the prediction of wave force is based on the past wave elevation, which can be measured easily with a wave probe fixed to a ground. Please note that for a floating WEC with horizontal motions, the position of the buoy should be known. However, it is out of the scope of the present research since the point-absorber is only allowed to oscillate vertically.

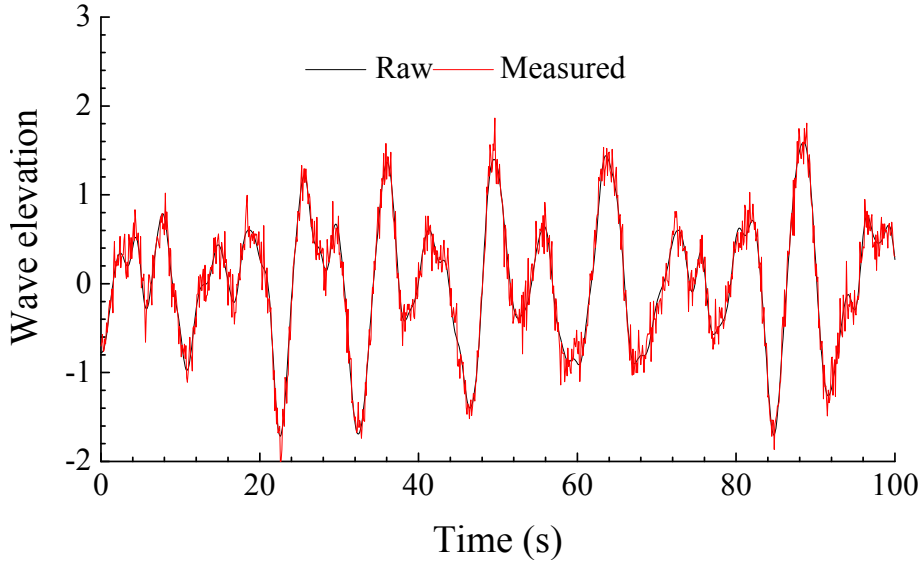

Fig. 5. Time histories of raw waves and measured waves.

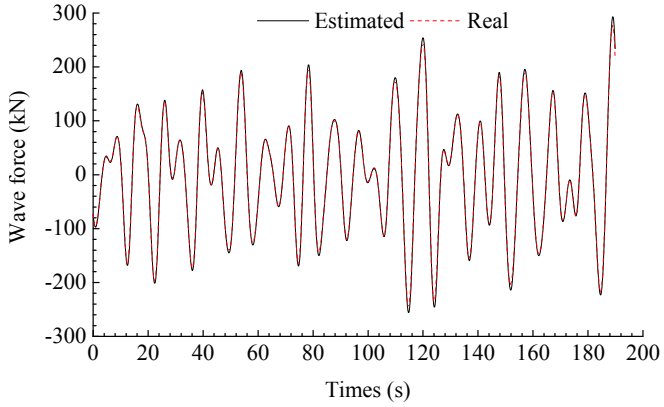

Fig. 6. Time series of the real and the estimated wave forces.

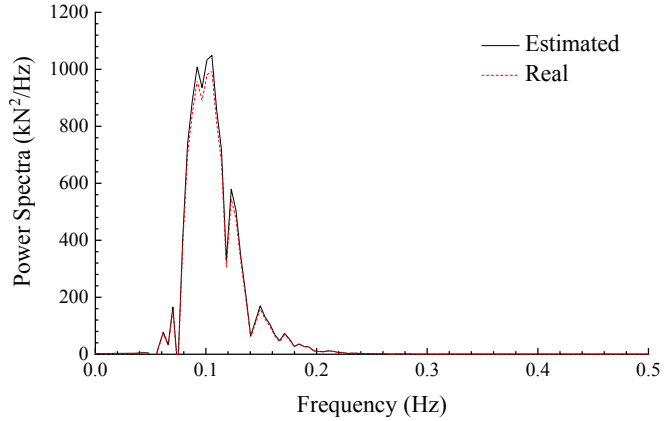

Fig. 7. Power spectra of the real and the estimated wave forces.

3.2. Generation of the training examples

In order to train the neural network, time series of wave elevations (input) and wave excitation forces (target) must be collected. The random wave elevations can be measured with a wave probe. Although we generate the wave elevations with numerical simulation in the present study, the uncertainty of wave elevation exists in the practical application due to the deviation of the wave probe and the wave noise. The wave noise is a complex physical phenomenon and depends on the sea site and the environment. The sensor deviation is determined by the hardware and is difficult to investigate theoretically. To focus on the present research, the wave uncertainty produced by the two factors altogether is simplified by adding a Gaussian-distribution noise to the raw elevations. The control input, namely the measured wave elevation with consideration of uncertainly produced by the two sources, is given by.

$$\widehat{\xi} = \xi + 0.15 \cdot \delta(0,1) \tag{17}$$

where $\widehat{\xi}$ is the measured wave elevation with noise and ξ is the raw wave elevation. $\delta(0,1)$ is a random value following the Gaussian distribution. Please note that Eq. (17) may not represent the real situation completely. Fig. 5 compares the measured wave elevation and the raw wave elevation.

In the actual case, the targeted wave forces F_{target} are nearly impossible to measure although they can be generated easily with a numerical model. Therefore, the wave forces must be estimated based on other measurable variables. We estimate the wave forces using the floater motion. The inverse function of Eq. (1) is

$$F_{target}(t) = \rho g \pi R^2 z(t) + z(t) + (C+B)\dot{z}(t) + (M+m)\ddot{z}(t) + \int_0^t H(t-\tau)\dot{z}(\tau)d\tau \tag{18}$$

Eq. (18) gives a way of estimating the wave forces by the floater motion. We don't use the inverse function of Eq. (10) because it is very difficult to value the state vector $\vec{u}(t)$ in an actual case. To check the uncertainty of the wave force estimation model, we first numerically generate time series of wave elevations and produce the wave forces according to Eq. (2). The generated wave forces are regarded as the real forces. Afterwards, the floater motion under the real wave forces are simulated with the state-space model. Based on the simulated floater motion, the estimation of wave forces is acquired by Eq. (18). Fig. 6 and Fig. 7 compare the estimated wave forces with the real values. Generally, the agreement is satisfactory despite some very slight discrepancies. Therefore, Eq. (18) is a reliable approach to acquire the training examples.

The forecasting of wave forces over the predictive horizon $[t, t+\Delta t]$ is based on the wave elevations in the past $[t-\Delta\tau, t]$, and the length of

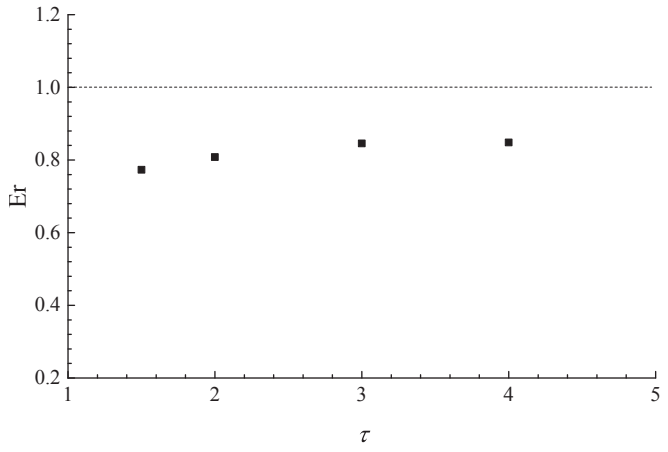

Fig. 8. Length of wave elevation points on the prediction performance.

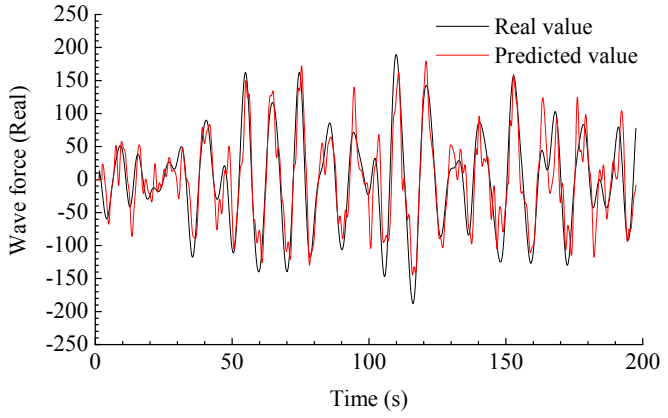

Fig. 9. Histories of predicted wave force 2.5 s ahead $\bar{f}(t+2.5|t)$with $\Delta\tau = 4.0$ s.

Table 1
Wave conditions.

	Case 1	Case 2	Case 3
H_s (m)	2	2.5	3
T_p (s)	1.2 T_n	1.6 T_n	2.0 T_n

collected wave elevations has an influence on the prediction performance. Consequently, we first seek the optimal ratio of Δt and $\Delta\tau$ to guarantee the best prediction performance. The predictability index in (Fusco and Ringwood, 2010) is used here to evaluate the prediction performance

$$Er = \frac{\int_0^T \bar{f}^2(t+\Delta t|t)dt}{\int_0^T f^2(t)dt} \tag{19}$$

where $f(t)$ is the wave force at time instant t; $\bar{f}(t+\Delta t|t)$ is the wave force Δt ahead predicted at time instant t. According to the definition, an index around 1 indicates good prediction performance. Fig. 8 demonstrates how the predictability index varies with the length of wave elevation collection. Generally, the prediction performance improves when a large number of wave elevation points are used to predict the future wave forces. Such variation trend is straightforward to understand since more information is collected for the prediction. When wave elevations over the past 4.0 s are collected for the forecasting, the predictability index is 0.8484.

The time series of predicted force $\bar{f}(t+\Delta t|t)$are plotted in Fig. 9. As shown, the prediction performance is satisfactory and thereby $\Delta\tau = 4.0$ s is used in the flowing part of this paper. It can be observed from Fig. 9 that the neural network is unable to predict the short-term wave force perfectly, due to the wave noise and the predicton algorithm itself. Since the control command is based on the predicted forces, the prediction deviation will have influences on the control performance. The following part will discuss this issue.

In the present research, three random wave states are considered, and three neural networks are trained to be applied in each sea state. It guarantees the best performance of the neural network. For example, if we train a neural network using wave data characterized by sea state *A* but apply it in sea state *B*, the prediction performance may be poor.

4. Simulation results

4.1. Energy conversion

In order to examine whether the real-time controller is effective in practice, we investigate its performance in random sea waves where the short-term wave forces are predicted with the neural network. Three sea states are selected and listed in Table 1, where $T_n = 5$ s is the natural period of the wave energy converter.

Fig. 10 plots the energy harvesting histories in the three wave conditions. When the point-absorber is free to oscillate in the random waves, the PTO system keeps producing power. Comparatively, the controlled energy harvesting is zero over some time intervals, when the floater is locked. Although the PTO system stops operating frequently due to the control action, the power extraction ramps rapidly as soon as the floater is set free. Fig. 11 compares the average energy absorptions with and without the controller. Generally, the point-absorber produces much more energy when the intelligent controller is active. It manifests that the smart controller can be successfully applied in practice. To estimate the efficiency of the present control algorithm, the power extraction with the complex conjugate control (representing the optimal mechanical power extraction) is also shown in Fig. 11. As shown, the heaving point-absorber generally converts 25% optimal energy with the present real-time latching control. Please note that it is assumed that the wave forces are fully known in the implementation of the complex conjugate control. A brief introduction of the complex conjugate control is given in the Appendix and please refer to (Falnes, 2002) for more details.

To interpret how the energy absorption is enhanced, the floater velocity is plotted in Fig. 12. As shown, the point-absorber is locked and released alternately. The floater is locked when the velocity vanishes. Once the floater is released, the velocity ramps rapidly. Furthermore, the controller velocity is closely associated with the wave forces. The floater is locked when the velocity and the wave forces are reverse and released again when they become aligned. In the meanwhile, the velocity and the wave forces nearly reach their maximum at the same time instant. It seems that the resonance is achieved with the real-time control. As stated before, the latching control is a kind of phase control, which increases the energy absorption by making the velocity in phase with the wave force. According to Fig. 12, the velocity and the wave force are indeed in phase. In this circumstance, the wave forces will always accelerate the floater so that it will carry more kinetic energy. As shown in Fig. 13, the wave forces sometimes slow down the floater without the real-time control since the work done on the floater is negative occasionally. When the floater motion is controlled, one can see that the wave excitation forces mostly do positive work to the floater.

4.2. Sensitivity of the energy conversion

4.2.1. Wave frequency

We first investigate how the control performance reacts to the wave frequency. Regular waves are considered here. Since the waves are regular, the wave forces over the time horizon are given rather than predicted here. The time horizon is set to $0.4\cdot(2\pi/\omega)$. The wave

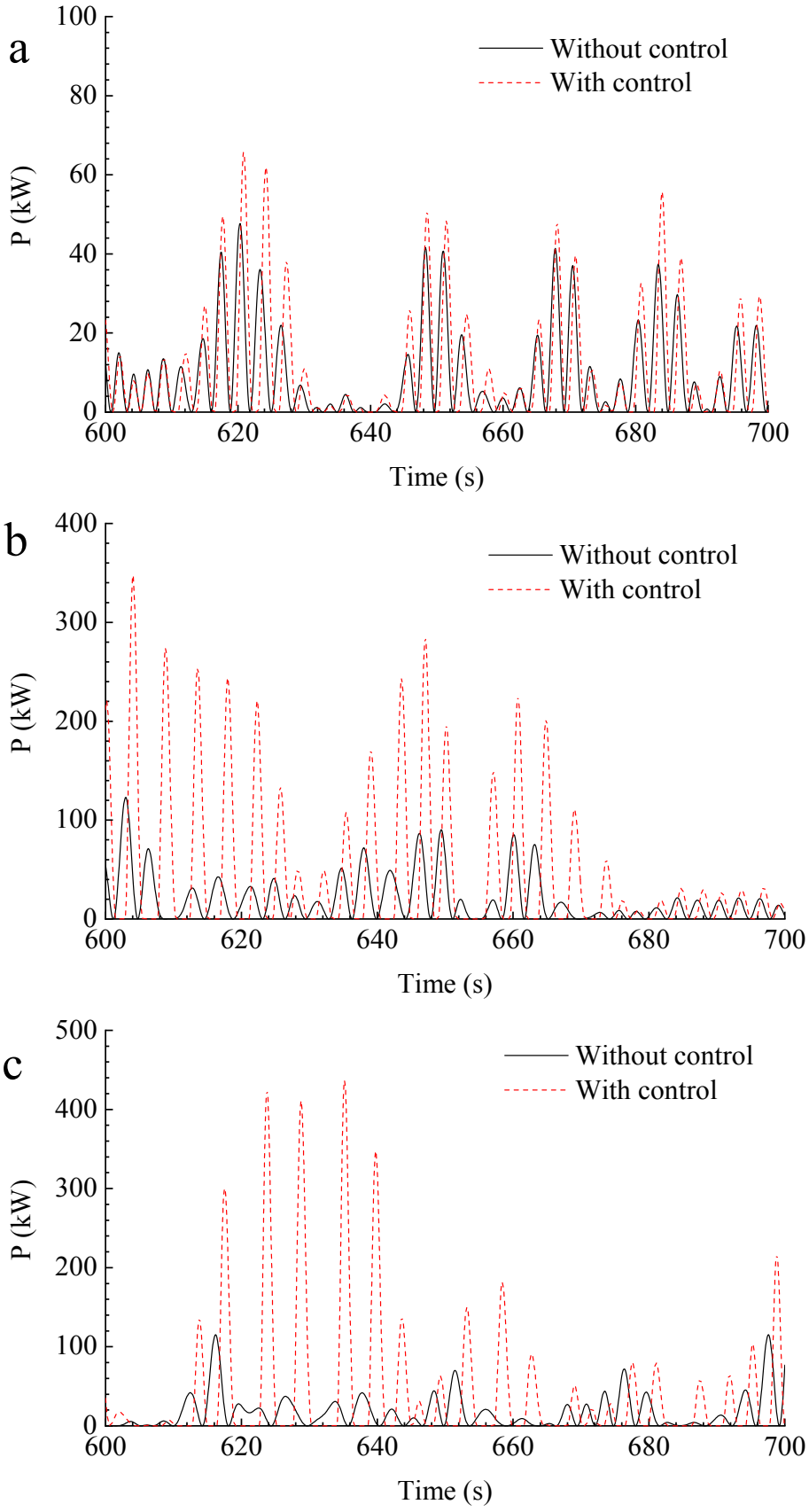

Fig. 10. Power capture histories. (a) Case1; (b) Case2; (c) Case3.

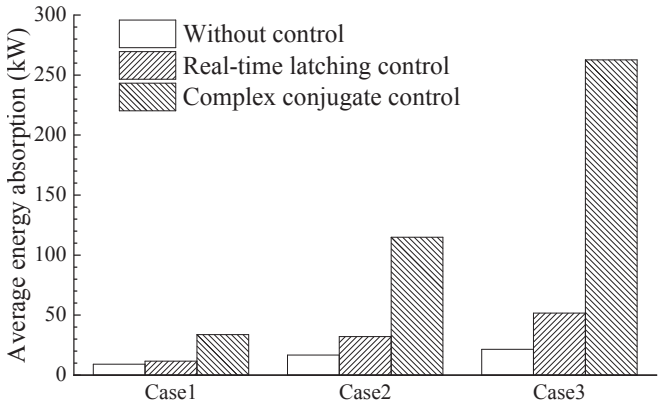

Fig. 11. Average energy harvesting.

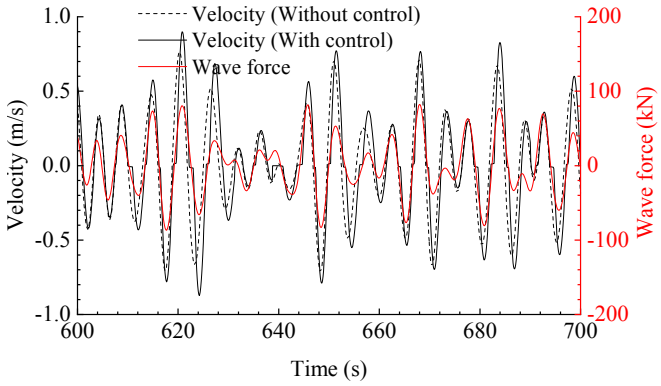

Fig. 12. Responses of the point-absorber, Case1.

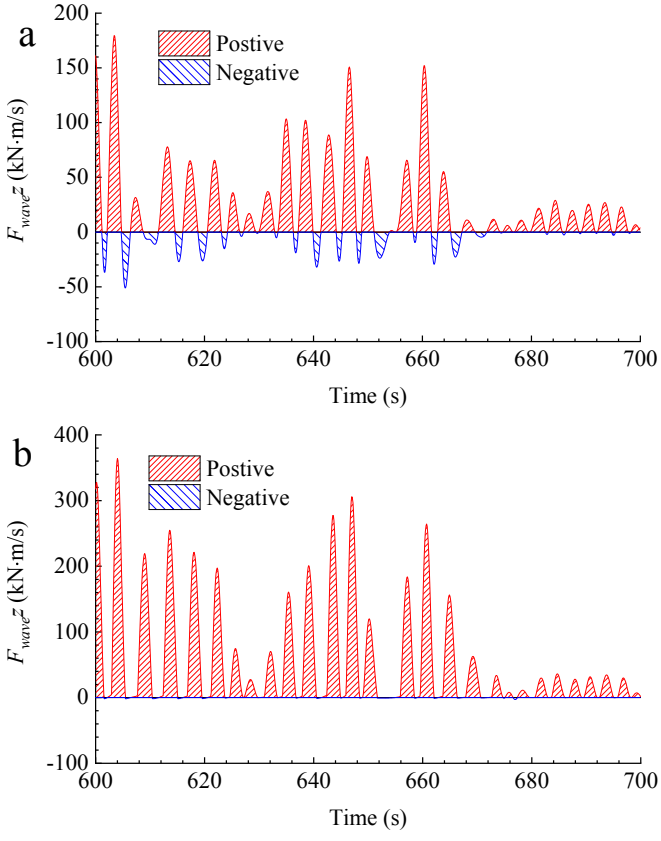

Fig. 13. Work on the floater done by the wave excitation force. Case1. (a) Without control; (b) With control.

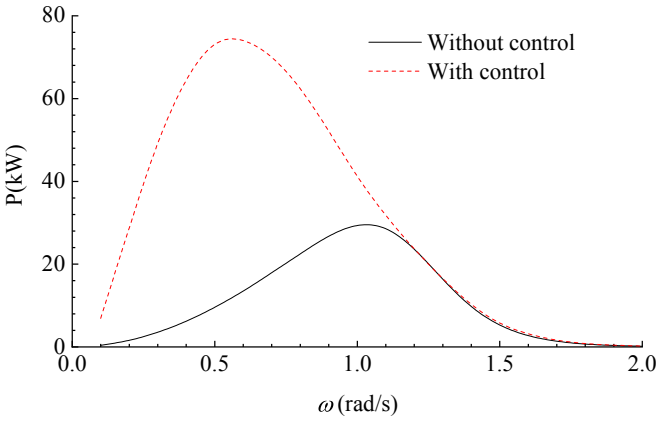

Fig. 14. Average energy absorption in regular waves.

amplitude is 1 m. Fig. 14 plots the sensitivity of energy absorption to wave oscillation frequency ω. Generally, the controller is effective over a wide of frequency range (0.1 rad/s to 1 rad/s). This range covers typical ocean waves spectrum so that the real-time control is effective in most cases. Nevertheless, the controller does not work at all within high-frequency range. Fig. 15 plots the time series of controlled motion and the wave excitation force. In long waves, the phase difference between the velocity and the wave forces are noticeable so that energy absorption can be enhanced by tuning the velocity phase. When the wave frequency is sufficiently high, the velocity is already in phase with the wave force. Therefore, it is useless to tune the phase and thereby the energy absorption is hardly varied on the right side in Fig. 14.

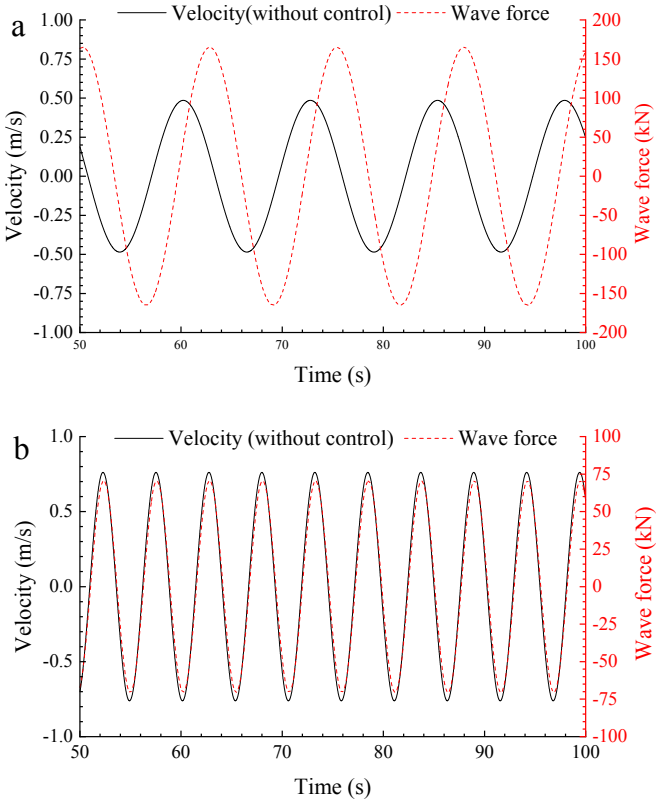

Fig. 15. Responses of the floater in regular wave. (a) $\omega = 0.5$ rad/s; (a) $\omega = 1.2$ rad/s.

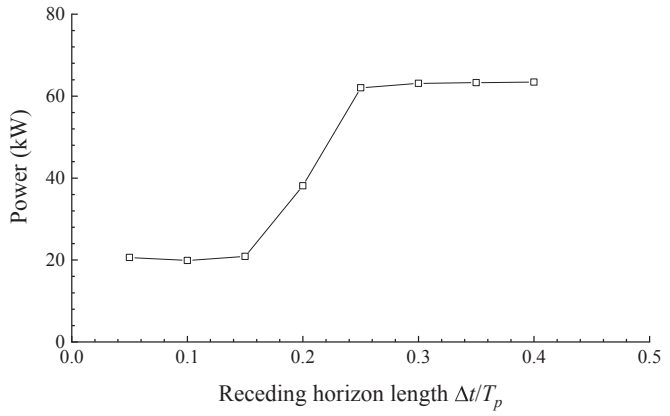

Fig. 16. Variation of energy absorption with receding horizon length, Case3.

4.2.2. Receding horizon length

To focus on the effect of receding horizon length, the wave force over the prediction time horizon is assumed already known to omit the prediction deviation. Fig. 16 illustrates how the average energy absorption varies with the length of the receding horizon. Three segments are identified within which the energy absorption shows different features. When the determination of control sequence is based on a short horizon length, the energy absorption remains relatively stable. In this segment, the control action is not effective at all as the energy absorption is identical to that without control. The performance of WEC is most sensitive to the horizon length within the middle segment. In this region, the energy absorption increases significantly with the receding horizon. As the horizon length continues increasing, the energy absorption gradually converges to a fixed level. Any further increase of receding horizon length has a very limited influence on the performance.

Fig. 17 illustrates how the receding horizon length influences the control command. When the length is very short, one can see that there is nearly no control action on the PTO system. For most of the moment, the floater is released. It is why the energy capture performance is very similar to that without control. As the length increases, the floater is latched more frequently indicating that the control action grows stronger. As a result, the energy absorption increases gradually. When the receding horizon length is long enough, the control command in Fig. 17 (c) and Fig. 17 (d) match well with each other. Consequently, the curve in Fig. 16 converges to a fixed level at the tail region.

4.3. Uncertainty of the energy conversion

As presented in Section 3.2, the measured wave elevations include noise. The discrepancies between the measured wave elevations and the real wave elevations may have an influence on the prediction performance. Even if we can remove the wave noise completely, the predicted wave forces are still not exact since we can't expect the neural network to perform perfectly. Therefore, two aspects of uncertainty affect the control performance. The first one is the uncertainty of control input. The second one is the prediction uncertainty, representing the forecasting capacity of the neural network. Fig. 18 shows the uncertainty effect on the control performance. The energy absorption is the largest when the uncertainty is removed. As plotted in Fig. 13, the wave forces occasionally do negative work to the floater due to the two aspects of uncertainties, so that the control efficiency is lower than the optimal level. Although the uncertainties have a negative influence on the control performance, the energy conversion is not reduced much. It implies that the smart controller can still work effectively in an actual case.

Wherever the uncertainties origin form, they ultimately lead to the prediction deviation and the differences in Fig. 18 can be interpreted by the prediction deviation. According to Eq. (2), the prediction deviation can be separated into two components, namely the amplitude deviation and the phase deviation. To demonstrate how the two components influence the control performance, we define the prediction deviation as following

$$\begin{aligned}\overline{F}_{amplitude}(t) &= \mathrm{Re}\left[\sum_{j=1}^{N} \alpha\psi(\omega_j)A_j e^{i\left(\omega_j t+\varepsilon_j\right)}\right]\\ \overline{F}_{phase}(t) &= \mathrm{Re}\left[\sum_{j=1}^{N} \psi(\omega_j)A_j e^{i\left(\omega_j t+\varepsilon_j+\theta_j\right)}\right]\end{aligned} \tag{20}$$

where $\overline{F}_{amplitude}$ are the defined wave forces involving only amplitude

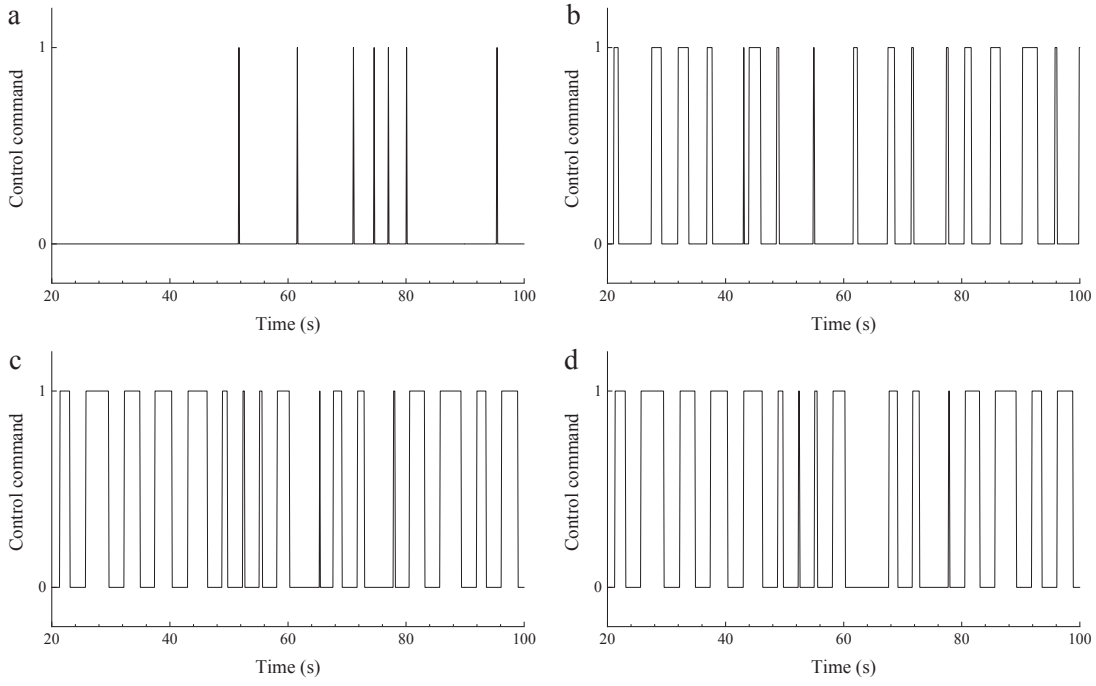

Fig. 17. Control command with various receding horizon lengths, Case3. (a) $\Delta t = 1.0$ s; (b) $\Delta t = 2.0$ s; (c) $\Delta t = 3.0$ s; (d) $\Delta t = 4.0$ s.

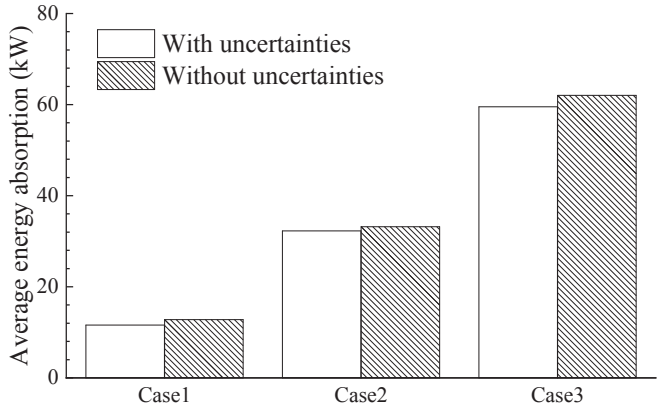

Fig. 18. Uncertainty effect on the energy absorption.

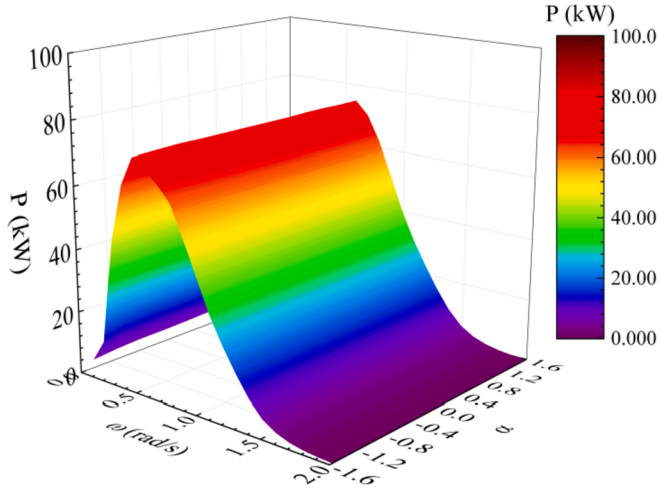

Fig. 19. Influence of amplitude deviation on the energy absorption.

deviation, $\overline{F}_{phase}$ are the defined wave forces involving only phase deviation. α and θ are parameters representing the level of amplitude and phase deviations, respectively. Eq. (20) reduces to Eq. (2) with $\alpha = 1$ and $\theta = 0$, meaning that the prediction deviation is eliminated. Such defined prediction deviation allows us to assess the phase deviation and the amplitude deviation separately. Please note that Eq. (20) is the input to the controller whereas the point-absorber is still subject to the real wave

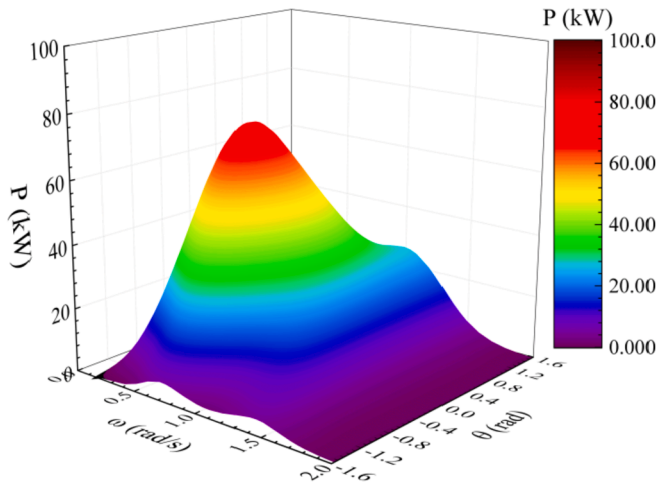

Fig. 20. Influence of phase deviation on the energy absorption.

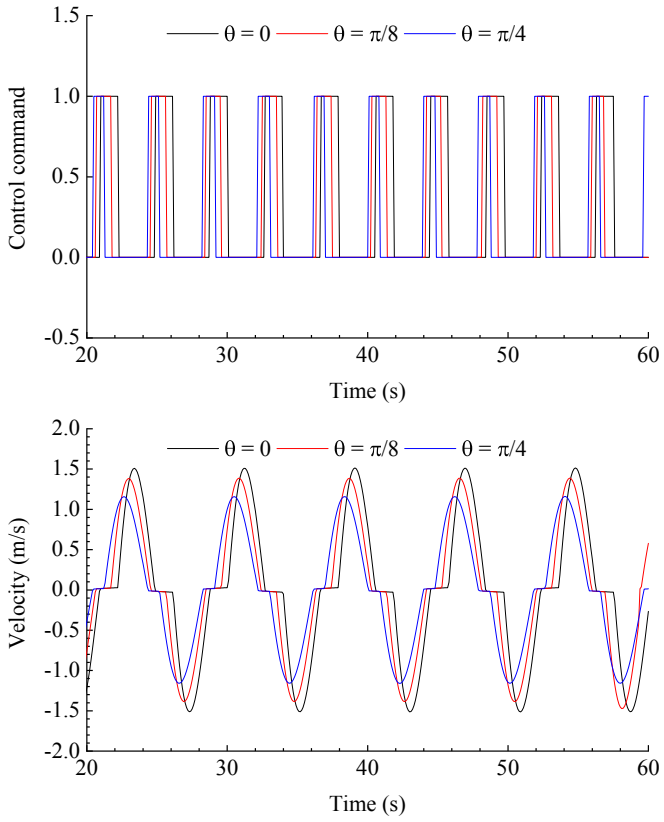

Fig. 21. Influence of phase deviation on energy absorption, $\omega = 0.8$ rad/s.

forces estimated by Eq. (2).

Fig. 19 demonstrates how the average energy absorption reacts to the amplitude deviation in regular waves. The energy absorption performance varies hardly with the amplitude deviation. It is not unexpected since the latching control is a kind of phase control so that the amplitude deviation is of minor importance.

Nevertheless, the phase deviation has a significant influence on the power extraction. As shown in Fig. 20, the power extraction drops considerably with the phase deviation θ. The average energy absorption drops significantly as the phase deviation amplifies. Fig. 21 interprets how the energy absorption drops with the phase deviation. When the phase deviation increases, the latched duration reduces indicating that the control action becomes weaker. In this circumstance, the velocity phase is not tuned sufficiently. Moreover, the latching action is applied earlier than it should be due to the phase deviation. It implies that the WEC is locked when it should be released. Due to these factors, the efficiency of the real-time control is reduced with the phase deviation.

5. Conclusions

A neural-network-based controller is developed in the present study to increase the energy efficiency of a heaving point-absorber. The controller adopts the model predictive control strategy to implement real-time latching control to the point-absorber. An artificial neural network is incorporated to predict the future wave forces based on the real-time measurement of wave elevations. In order to acquire the wave forces which are unable to measure directly, a numerical model is developed to estimate the wave forces based on floater motions. The estimated forces are adopted as the training examples.

The controller enhances the energy efficiency by locking and releasing the floater alternately. In this way, the velocity is tuned and becomes in phase with the wave forces. Therefore, the wave forces will always accelerate the floater.

The energy conversion is sensitive to wave frequency and the length of receding horizon. The energy absorption is only increased on condition that the wave frequency is sufficiently low. Furthermore, the wave energy converter absorbs more power if a longer receding horizon is applied.

Due to uncertainties produced by the wave noise and the prediction algorithm itself, the prediction deviation is unavoidable. The prediction deviation has a negative effect on the control performance since the control command is derived based on the inaccurate wave forces. It is found that amplitude deviation has a very limited influence on the control efficiency. It is the phase deviation that reduces the energy efficiency. In the presence of phase deviation, the floater is locked and released at wrong time instants.

The present research just considers one degree of freedom (DoF) and the buoy is only allowed to oscillate vertically. In real practice, a WEC is typically positioned using mooring lines and the 6-DoF motions should be considered. The WEC converts the wave-frequency heave motion, which is hardly influenced by the mooring system, into the electricity power. Therefore, the 1-DoF assumption in the present research still makes sense. Nevertheless, the 6-DoF motions should be considered in the prediction of the future wave forces. More specifically, the horizontal motions (surge and sway) of the buoy should be known. This can be achieved in practice with several approaches, e.g. the GPS.

Acknowledgement

The first author is grateful for the financial support from ETP PECRE (Grant No. PECRE31).

Appendix

The frequency-domain motion equation of the heaving point-absorber with unit wave amplitude is given by

$$Z(\omega)u(\omega) = F_{wave}(\omega) + F_{PTO}(\omega)$$

where u is the velocity. F_{wave} and F_{PTO} are the wave force and the mechanical force of the PTO, respectively. Z is the intrinsic impedance of the buoy

$$Z(\omega) = \lambda(\omega) + B + i\omega(M + \mu(\omega)) + \frac{\rho g \pi R^2}{i\omega}$$

where λ is the radiation damping and μ is the added mass. B is the additional damping coefficient defined in Section 2.1. Fig. 22 plots the intrinsic impedance of the buoy.

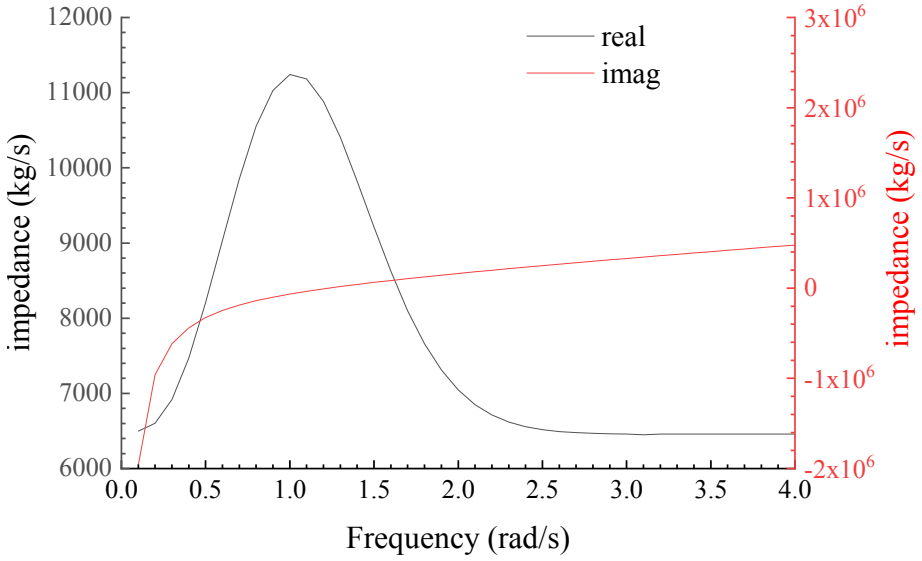

Fig. 22. Intrinsic impedance of the buoy.

According to (Falnes, 2002), the optimal condition for the power extraction is

$$u(\omega) = \frac{1}{2}\mathrm{Re}\{Z(\omega)\}^{-1}F_{wave}(\omega)$$

$$F_{PTO}(\omega) = -\frac{1}{2}Z^*(\omega)\cdot\mathrm{Re}\{Z(\omega)\}^{-1}F_{wave}(\omega)$$

where Z^* is the complex conjugate of Z. Then the optimal average power absorbed is

$$P = \frac{1}{2\pi}\int_0^\infty \frac{|f(\omega)|^2}{2\mathrm{Re}\{Z(\omega)\}}d\omega$$

where $f(\omega)$ is the Fourier transform of the wave excitation $F_{wave}(t)$. Given the wave spectrum $S(\omega)$ and the wave force transfer function $\psi(\omega)$, $f(\omega)$ can be expressed analytically as

$$f(\omega) = e^{iW(\omega)} \cdot \psi(\omega) \cdot \sqrt{\pi S(\omega)}$$

where $W(\omega)$ is a random value between 0 and 2π. $e^{iW(\omega)}$ represents the random phase of each component.

Please note that $\left|e^{iW(\omega)}\right| = 1$ and thereby the optimal average power extraction is given by

$$P = \frac{1}{4}\int_0^\infty \frac{|\psi(\omega)|^2 S(\omega)}{\mathrm{Re}\{Z(\omega)\}} d\omega$$

References

Babarit, A., Clement, A.H., 2006. Optimal latching control of a wave energy device in regular and irregular waves. Appl. Ocean Res. 28 (2), 77–91.

Babarit, A., Guglielmi, M., Clement, A.H., 2009. Declutching control of a wave energy converter. Ocean Eng. 36 (12–13), 1015–1024.

Boltyanskiĭ, V.G., Gamkrelidze, R.V., Pontryagin, L.S., 1956. On the theory of optimal processes. Dokl. Akad. Nauk SSSR 110, 7–10.

Budal, K., Falnes, J., 1980. Interacting point absorbers with controlled motion. In: Power from Sea Waves. BM Count. Academic Press.

Cummins, W., 1962. The Impulse Response Function and Ship Motions. David Taylor Model Basin, Washington DC, pp. 101–109.

Elhanafi, A., Macfarlane, G., Fleming, A., Leong, Z., 2017. Experimental and numerical investigations on the hydrodynamic performance of a floating moored oscillating water column wave energy converter. Appl. Energy 205, 369–390.

European Marine Energy Centre, 2018. AQUAMARINE POWER. http://www.emec.org.uk/about-us/wave-clients/pelamis-wave-power/.

European Marine Energy Centre, 2018. Pelamis Wave Power. http://www.emec.org.uk/about-us/wave-clients/pelamis-wave-power/.

Evans, D.V., Jeffrey, D.C., Salter, S.H., Taylor, J.R.M., 1979. Submerged cylinder wave energy device: theory and experiment. Appl. Ocean Res. 1 (1), 3–12.

Falnes, J., 2002. Ocean Waves and Oscillating Systems: Linear Interactions Inlcuding Wave-Energy Extraction. Cambridge University Press.

Fusco, F., Ringwood, J.V., 2010. Short-term wave forecasting for real-time control of wave energy converters. IEEE Transactions on Sustainable Energy 1 (2), 99–106.

Fusco, F., Ringwood, J., 2011. A model for the sensitivity of non-causal control of wave energy converters to wave excitation force prediction errors. In: Proceedings of the 9th European Wave and Tidal Energy Conference (EWTEC). School of Civil Engineering and the Environment, University of Southampton.

Ge, M., Kerrigan, E.C., 2016. Short-term ocean wave forecasting using an autoregressive moving average model. In: 11th International Conference on Control. IEEE, Belfast, UK, pp. 1–6.

Halliday, J.R., Dorrell, D.G., Wood, A.R., 2011. An application of the Fast Fourier Transform to the short-term prediction of sea wave behaviour. Renew. Energy 36 (6), 1685–1692.

Henriques, J.C.C., Gato, L.M.C., Falcao, A.F.O., Robles, E., Fay, F.X., 2016. Latching control of a floating oscillating-water-column wave energy converter. Renew. Energy 90, 229–241.

Kalogirou, S.A., 2001. Artificial neural networks in renewable energy systems applications: a review. Renew. Sustain. Energy Rev. 5 (4), 373–401.

Li, L., Yuan, Z., Gao, Y., Zhang, X., 2018. Wave force prediction effect on the energy absorption of a wave energy converter with real-time control. IEEE Transactions on Sustainable Energy 10 (2), 615–624, 1-1.

Margheritini, L., Vicinanza, D., Frigaard, R., 2009. SSG wave energy converter: design, reliability and hydraulic performance of an innovative overtopping device. Renew. Energy 34 (5), 1371–1380.

Perez, T., Fossen, T.I., 2011. Practical aspects of frequency-domain identification of dynamic models of marine structures from hydrodynamic data. Ocean Eng. 38 (2), 426–435.

Salter, S.H., 1974. Wave power. Nature 249 (5459), 720–724.

Sclavounos, P.D., Ma, Y., 2018. Artificial intelligence machine learning in marine hydrodynamics. In: 37th International Conference on Ocean. Offshore and Arctic Engineering, Madrid, Spain. V009T013A028.

Sclavounos, P.D., Ma, Y., 2018. Wave energy conversion using machine learning forecasts and model predictive control. In: 33st International Workshop on Water Waves and Floating Bodies, Brest, France.

Smith, B.L., Demetsky, M.J., 1994. Short-term traffic flow prediction models-a comparison of neural network and nonparametric regression approaches. Proc. IEEE Int. Conf. Syst. Man Cybern. 1706–1709.

Son, D., Yeung, R.W., 2017. Optimizing ocean-wave power extraction of a dual coaxial-cylinder WEC using nonlinear model predictive control. Appl. Energy 187, 746–757.

Son, D., Yeung, R.W., 2017. Real-time implementation and validation of optimal damping control for a permanent-magnet linear generator in wave power extraction. Appl. Energy 208, 571–579.

Taghipour, R., Perez, T., Moan, T., 2008. Hybrid frequency-time domain models for dynamic response analysis of marine structures. Ocean Eng. 35 (7), 685–705.

United States Department of Energy, 2015. Innovative Wave Power Device Starts Producing Clean Power in Hawaii. https://www.energy.gov/eere/articles/innovative-wave-power-device-starts-producing-clean-power-hawaii/.

Williams, P., 2004. Application of pseudospectral methods for receding horizon control. J. Guid. Control Dyn. 27 (2), 310–313.

Yu, F., Xu, X.Z., 2014. A short-term load forecasting model of natural gas based on optimized genetic algorithm and improved BP neural network. Appl. Energy 134, 102–113.

Zhang, X.T., Yang, J.M., Zhao, W.H., Xiao, L.F., 2016. Effects of wave excitation force prediction deviations on the discrete control performance of an oscillating wave energy converter. Ships Offshore Struct. 11 (4), 351–368.